Solution Structure of the hDlg/SAP97 PDZ2 Domain and Its Mechanism of Interaction with HPV-18 Papillomavirus E6 Protein[†,‡]

Yuqi Liu,[§] Gillian D. Henry,[§] Rashmi S. Hegde,[||] and James D. Baleja*[,§]

Department of Biochemistry, Tufts University School of Medicine, 136 Harrison Avenue, Boston, Massachusetts 02111, and Division of Developmental Biology, Cincinnati Children's Hospital Medical Center, 3333 Burnett Avenue, Cincinnati, Ohio 45229

Received May 9, 2007; Revised Manuscript Received July 12, 2007

ABSTRACT: The E6 protein from high-risk types of human papillomavirus (HPV) binds PDZ-domain containing proteins and targets them for degradation. We used isothermal titration calorimetry to measure the interaction of a peptide from the C-terminus of HPV-18 E6 to the second PDZ domain (PDZ2) from the human homologue of the *Drosophila* discs large tumor suppressor protein (hDlg). Isothermal titration calorimetry experiments with a series of peptides showed that HPV-18 E6 bound hDlg PDZ2 about 5-fold stronger than HPV-16 E6, that the contribution of Arg154 to binding was about 1 kcal/mol, and that the binding was disabled by phosphorylation at Thr156. We then used NMR to determine the solution structure of the complex of PDZ2 bound to the HPV-18 E6 peptide. The resultant structures were of high quality and had backbone root-mean-square deviations of less than 0.5 Å. The structure shows a novel mode of interaction in which six residues of the HPV-18 E6 peptide are contacted by the PDZ2 domain, in contrast to the typical four residues used by class I PDZ domains. Molecular dynamics simulations supported a model in which the C- and N-terminal ends of the peptide had different mobilities within the complex. Comparison of the NMR complex structure to previously determined X-ray structures of PDZ2 by itself and bound to different peptides allows a description of conformational changes required for PDZ2 to bind to HPV-18 E6.

Papillomaviruses are small double stranded DNA viruses that infect both mucosal and cutaneous epithelial tissues. High-risk human papillomavirus (HPV[1]) is strongly associated with the development of malignant lesions and promote cervical cancer in over 95% of cases (*1*). HPV-16 and HPV-18 are the most common types in invasive cervical squamous cell carcinomas, accounting for over 65% of these cancers. HPV-18 is the predominant type in cervical adenocarcinomas, followed by HPV-16 (*2*, *3*). The E6 protein is multifunctional, and many cellular targets have been identified. The most extensively studied function of E6 is complex formation with the cellular E6-associated ubiquitin ligase protein (E6AP), which subsequently targets p53 for degradation, thereby preventing the cell apoptosis associated with viral infection (*4*). HPV E6 also possesses p53-independent functions, which are also necessary for transformation. Numerous E6-interacting proteins harbor PDZ (PSD95/Discs Large/ZO-1) domains including a human homologue of the *Drosophila* discs large tumor suppressor protein (hDlg, also known as SAP-97) (*5*, *6*), a human homologue of the *Drosophila* scribble tumor suppressor protein (hScrib) (*7*) and others (*8*−*10*). Like the degradation of p53 (*11*), these PDZ proteins have been shown to be targeted by E6AP-dependent, proteasome-mediated degradation (*7*−*10*, *12*−*15*).

The high-risk HPV E6 proteins deregulate aspects of cell growth and polarity in response to cell contact through the degradation of hDlg (*5*, *6*, *12*−*14*). E6 mutants losing the ability to bind to hDlg are no longer able to induce E6-dependent transformation of rodent cells (*5*). These results suggest that interaction between the E6 protein and hDlg or other PDZ domain-containing proteins is an underlying mechanism in the development of HPV-associated cancers. PDZ binding motifs have been identified in several virus proteins associated with oncogenesis, including the HTLV-1 Tax protein (*16*), the adenovirus 9 E4-ORF1 protein (*8*, *9*), and the high-risk HPV E6 proteins (*5*, *6*, *12*−*14*). The commonality of binding to oncogenic virus proteins indicates that the PDZ proteins represent conserved pathways that are subverted during oncogenic transformation.

The hDlg protein contains three PDZ domains which have been evaluated separately for their ability to bind diverse recognition sequences including those from HPV E6 (*5*), adenovirus E4 ORF1 (*6*), adenomatous polyposis coli (APC)

[†] Supported in part by NIH Grant AI38001.

[‡] Atomic coordinates have been deposited with the Research Collaboratory for Structural Bioinformatics Protein Databank, filename 2OQS, and NMR assignments have been deposited at the BioMagResBank (BMRB) NMR structural database, accession number 15209.

* To whom correspondence should be addressed. Phone: (617) 636-6872. Fax: (617) 636-2409. E-mail: jim.baleja@tufts.edu.

[§] Tufts University School of Medicine.

[||] Cincinnati Children's Hospital Medical Center.

[1] Abbreviations: C8E5, pentaethylene glycol *n*-octyl ether; DDM, distance difference matrix; hDlg/SAP, human homologue of the *Drosophila* discs large tumor suppressor protein; HPV, human papillomavirus; HSQC, heteronuclear single quantum coherence; ITC, isothermal titration calorimetry; NOE, nuclear Overhauser effect; NOESY, NOE spectroscopy; PDZ, postsynaptic density protein/disc large/zonula occludens; rms, root-mean-square; TCEP, tris(2-carboxyethyl)phosphine; TOCSY, total correlated spectroscopy.

10.1021/bi700879k CCC: $37.00
Published on Web 08/22/2007

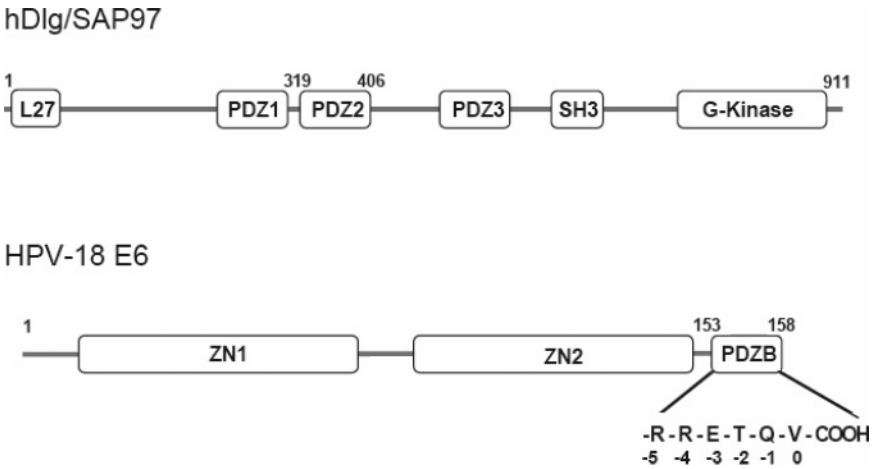

FIGURE 1: Domain representations of hDlg/SAP97 and HPV-18 E6 proteins. The hDlg protein has an L27 domain at its N-terminus, which is involved in protein−protein interactions, three PDZ domains (PDZ1, PDZ2, and PDZ3), an SH3 domain, and a C-terminal region with homology to GTP kinases (*74*). The E6 protein has two zinc-binding domains (ZN1 and ZN2) and a PDZ-binding motif (PDZB). The PDZ-binding motif, RRETQV, is shown and numbered relative to the last residue below the amino acid sequence.

(*17*), and *N*-methyl-D-aspartate receptor 2 B unit (NR2B) (*18*). In general, the second PDZ domain (PDZ2) appears to have the strongest affinity, whereas PDZ1 has weaker affinity and PDZ3 shows even less binding (*5*, *6*, *17*−*19*).

The presence of the PDZ-binding motif in the E6 protein of the high-risk HPV types, but not low-risk HPV types, suggests a role in HPV-induced oncogenesis (*6*, *21*). Some HPV E6 proteins that have mutations at the C-terminus lose the ability to bind PDZ domain proteins but retain the ability to inactivate p53, indicating that E6 contributes to cancer through disruption of two cellular pathways, one of which is mediated through interaction with PDZ domain partners and the other through the inactivation of p53 (*22*). The canonical binding mode of class I PDZ interactors (which have the sequence -x-S/T-x-Φ, where Φ is a hydrophobic amino acid) predicts that high-risk HPV E6 proteins bind to PDZ-containing proteins using only the last four residues in their carboxyl termini (x-S/T-x-V/L) (*20*). Analysis of the C-termini of E6 proteins of high-risk HPV types shows a conserved consensus protein kinase A (PKA) recognition site (Rxx[S/T] or Rx[S/T]) that overlaps with the PDZ-binding motif (except in HPV-73). In the case of HPV-18 E6, the sequence is R_{153}-R_{154}-E_{155}-T_{156}-Q_{157}-V_{158} (Figure 1). The PKA site does not overlap with the predicted PDZ-binding motifs in E6 of "probable" high-risk HPV types (HPV-26, -53, and -66), and does not occur in other virus proteins (*8*, *9*, *16*, *18*, *23*). Thr156 at the p-2 position of HPV-18 E6 is critical for *in vitro* binding to hDlg, as mutation to either other neutral or acidic amino acids abolishes binding (*13*). Stimulation of PKA activity inhibits HPV-18 E6-induced degradation of hDlg, but not of p53 (*24*), and the mutation of the conserved arginine at the p-5 position abrogates PKA's negative regulation (*25*). In the absence of structural data, how HPV E6 proteins bind to the hDlg PDZ domain is not clear, particularly the roles of the two highly conserved Arg residues of E6 in the complex.

Structures for each of the PDZ domains of hDlg in the absence of HPV E6 have been reported. They include the NMR structure of the first PDZ domain in complex with NR2B peptide (*18*), the crystal structures of the second PDZ domain unbound and bound to a peptide from the GluR-A protein (*26*), and the crystal structure of the third PDZ domain alone (*27*). Structures of hDlg PDZ2 homologues unbound to peptides have also been reported (*28*). The observed structures show a typical PDZ architecture, and contain six β-strands and two α-helices (*27*, *29*−*31*). The C-terminal three or four residues of target proteins form a short β strand that binds in a groove formed by the long α-helix and the second β-strand and antiparallel to the strand (*29*, *31*).

To investigate the binding mechanism between hDlg and HPV E6 protein in solution, we determined the NMR structure of hDlg PDZ2 in complex with the C-terminus sequence of high-risk HPV E6. The structure of the complex reveals the interface of hDlg PDZ2 domain binding to E6 protein, which provides a platform for understanding the molecular basis of the binding specificity between hDlg PDZ domains and HPV E6. A novel binding mode for PDZ-peptide recognition was found in which the C-terminal six amino acids of HPV E6 were in contact with the PDZ domain. Our solution experiments also provide dynamic information associated with binding.

In the final stages of preparation of this manuscript, crystal structures of three PDZ domains each in complex with a seven amino acid peptide from HPV-18 E6 were independently reported (*32*). Combining our solution structure, chemical exchange measurements, and titration experiments with the crystallographic study provides a more accurate picture of the binding mechanism between hDlg PDZ domains and HPV E6 and includes the roles of particular amino acids used for binding and in dynamics.

MATERIALS AND METHODS

Protein Expression and Purification. The DNA encoding the second PDZ domain of human hDlg (residues 318−405) was cloned between the *Nde*I and *Bam*HI sites of the pET30a(+) vector. The protein construct contained an additional N-terminal methionine and a C-terminal glycine-serine linker connecting to a hexahistidine tag. The transformed BL21(DE3) cells were grown at 37 °C to OD_{600} of 0.8 before induction with 0.4 mM isopropyl 1-thio-β-D-galactopyranoside overnight. Isotopically enriched (^{15}N, ^{13}C, and $^{15}N/^{13}C$) samples were prepared by growing cells in

modified M9 medium containing $^{15}NH_4Cl$ and/or [^{13}C]-glucose and the corresponding Celtone (1 g/L) (*33*). Cells were lysed by sonication, and the protein was purified with a HiTrap chelating HP column (Amersham Pharmacia Biotech), followed by elution with 100 mM imidazole (pH 8.0). The protein was further purified by gel filtration on Sephadex G75 in 20 mM sodium phosphate (pH 6.5). The pooled fractions were concentrated to ~2 mM, aliquoted, and lyophilized. A sample for NMR was prepared by redissolving a lyophilized aliquot and rechecking its pH value.

Peptide Design. Four peptides containing the C-terminus of HPV-18 E6 sequence (acetyl-RRETQV-[COOH], hereafter called E6CT), the C-terminus of HPV-16 E6 sequence (acetyl-RRETQL-[COOH], E6CT0L), the Thr156-phosphorylated C-terminus of HPV-18 E6 (acetyl-RRE$_p$TQV-[COOH], E6CT2p), and an Arg154Gly mutant peptide (acetyl-RGETQV-[COOH], E6CT4G) were designed to investigate the roles of particular amino acid residues in binding. Peptides were synthesized using FMOC chemistry and purified by C_{18} reversed-phase high-performance liquid chromatography (HPLC). Identities were confirmed using matrix-assisted laser desorption ionization (MALDI) mass spectrometry.

Isothermal Titration Calorimetry. ITC experiments were performed using a VP-ITC system (MicroCal) at 20 °C in 20 mM phosphate buffer (pH 6.5). Proteins were dialyzed against buffer, centrifuged, and degassed before the experiment. Typically, a 200 μM peptide solution was injected 30 times in 10 μL aliquots into the 1.4 mL sample cell containing hDlg PDZ2 domain at a concentration of 10 μM. For E6CT0L, the PDZ2 and peptide concentrations were adjusted to 50 μM and 1.0 mM, respectively. Data were fit with a nonlinear least-squares routine using a single-site binding model with Origin for ITC v.7.0 (Microcal), varying the stoichiometry (n), the enthalpy of the reaction (ΔH), and the association constant (K_a).

NMR Spectroscopy. All NMR experiments were acquired at 20 °C on a Bruker Avance-600 spectrometer. Uniformly ^{15}N-labeled PDZ2 domain (0.33 mM) was titrated with E6CT peptide from 10 mM stocks. $^1H-^{15}N$ HSQC spectra were collected at peptide:protein molar ratios of between 0 and 4.5. Residues for which the intensity remained strong throughout the titration were classified as being in fast exchange if they showed a continuous chemical shift change and in slow exchange if they showed only either the unbound resonance or the bound resonance. Other residues for which the intensity disappeared during the midpoint of the titration were designated as being in intermediate exchange. For residues in fast exchange, the observed chemical shift change was fitted using the following equation (*34*):

$$\Delta\delta = (\Delta\delta_{max})\{L_0 + P_0 + K_d - [(L_0 + P_0 + K_d)^2 - 4L_0P_0]^{1/2}\}/2P_0 \quad (1)$$

where $\Delta\delta$ is the chemical shift change, $\Delta\delta_{max}$ is the chemical shift change at saturation, L_0 is the total peptide concentration, P_0 is the total protein concentration, and K_d is the equilibrium dissociation constant. A K_d value was determined by nonlinear least-squares fitting of eq 1 of $\Delta\delta$ *versus* the two independent variables L_0 and P_0 using OriginLab software.

For structure determination, samples were about 2 mM in 20 mM phosphate (pH 6.5) and 4 mM Tris(2-carboxyethyl)-phosphine (TCEP). Resonance assignments and NOE analyses were performed on a $^{15}N,^{13}C$ protein sample using a suite of pulsed-field gradient-enhanced NMR experiments as described (*35*, *36*). Briefly, resonance assignment was carried out using standard homonuclear 2D NMR experiments and a series of double- and triple-resonance experiments, including 2D $^1H,^{15}N$-HSQC and $^1H,^{13}C$-HSQC, 3D $^1H,^{15}N$ TOCSY-HSQC and NOESY-HSQC, HN(CA)CO, HNCACB, CBCACONH, and HCCH-TOCSY spectra (*37*−*42*). $^1H-^{15}N$ residual dipolar couplings were measured in C8E5/*n*-octanol alignment media (*43*), using a molar ratio of C8E5/*n*-octanol of 0.87 and a C8E5/water ratio of 5 wt %, in 20 mM phosphate buffer (pH 6.5) with 10% D_2O. Samples using 10 to 15 mg/mL of filamentous bacteriophage Pf1 as the alignment medium had poor spectral quality and were not analyzed further. Stereospecific assignments of valine and leucine methyl groups were obtained from a constant-time (CT) $^1H-^{13}C$ HSQC spectrum acquired on a 10% ^{13}C-labeled sample (*44*, *45*). To obtain unambiguous intermolecular NOEs, a 2D ^{13}C-filtered,$^{13}C,^{15}N$-filtered NOESY spectrum was recorded (*46*). All data were processed with Bruker XWINNMR. SPARKY was used for resonance assignment and to measure NOE cross-peak intensities (*47*).

Conformational Data and Structure Calculations. NOEs for structure calculation were measured from a 2D NOESY spectrum collected in D_2O and from a 3D $^1H-^{15}N$-NOESY-HSQC spectrum in H_2O using a mixing time of 100 ms. Backbone dihedral angle restraints were derived from the secondary structure of the protein and the backbone chemical shift analysis program TALOS (*48*). For amide protons protected from exchange with D_2O (Table S1), hydrogen bond restraints were set with 1.6 Å < d_{NH-O} < 2.4 Å and 2.4 Å < d_{N-O} < 3.5 Å using the acceptor identified from initial rounds of structure calculation. Structures were calculated using the CNS program (version 1.1) (*49*) as described (*50*). The NOE/hydrogen bond and dihedral constraints used the default force constants (75 kcal/Å^2 and 400 kcal/deg^2, respectively). The E_{repel} function was replaced by a Lennard-Jones potential during the final Powell minimization. Ten initial structures of the complex were calculated without the residual dipolar coupling restraints. Alignment tensor parameters (D_a and R) were determined using PALES (*51*). The residual dipolar coupling restraints were incorporated into the final calculation with a force scale from 0.1 to 50 in Cartesian space. The resulting 30 structures were validated by PROCHECK (*52*) and WHATIF (*53*) programs. Structural statistics were performed with PROCHECK (*52*). Hydrogen bonds were identified if present in the majority of calculated structures. Structures were compared by using ESCET scripts (*54*).

Molecular Dynamics. Molecular dynamics simulations were performed with the parallel molecular dynamics program NAMD (*55*) using the CHARMM22 force field (*56*). The mean structure of the 30 calculated NMR structures was generated for a starting point. After placing the structure inside a water sphere, solvent molecules were relaxed by using 1000 steps of energy minimization at 310 K. Minimized coordinates were then used for 20 ps molecular dynamics (MD) runs at 278, 310, 380, and 450 K, respectively. The electrostatic interaction between 1 and 4 atoms

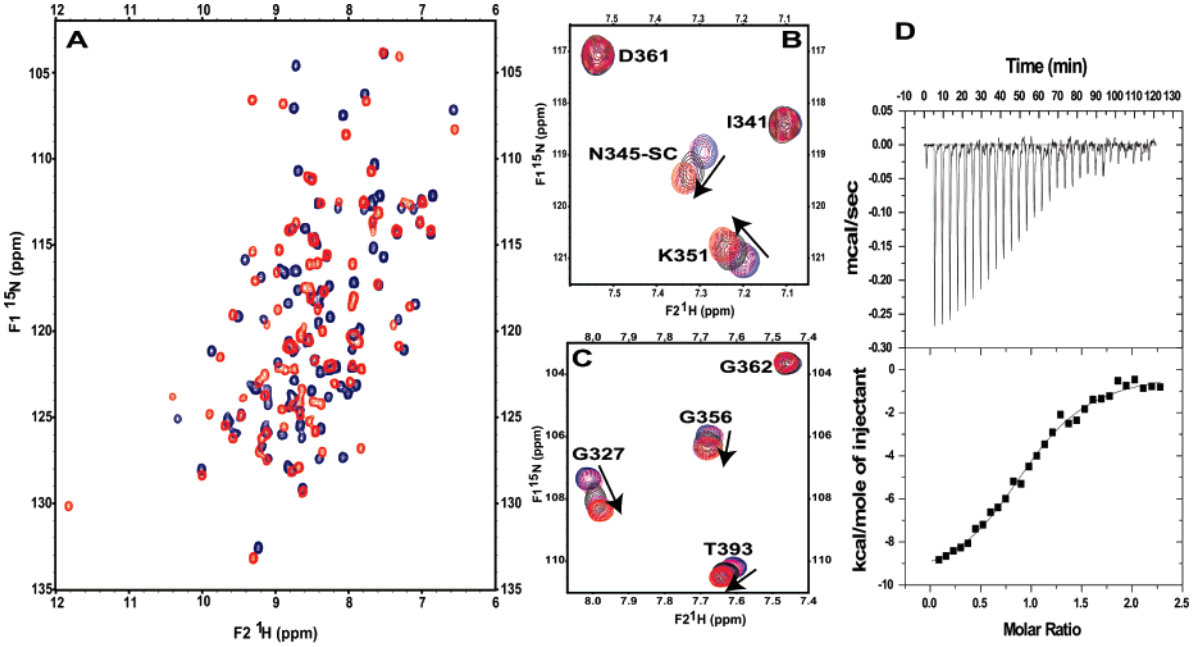

FIGURE 2: Binding of the E6CT peptide to the hDlg PDZ2 domain by NMR spectroscopy and ITC. (A) $^{1}H-^{15}N$ HSQC spectrum of ^{15}N-labeled PDZ2 domain in the absence (blue contours) and presence (red contours) of 1.5× unlabeled E6CT peptide. (B, C) The chemical shift changes of selected residues showing fast exchange. (D) Analysis of the interaction of hDlg PDZ2 domain and E6CT peptide by ITC in 20 mM phosphate (pH 6.5).

was taken into account. A cutoff of 12 Å was set for electrostatic and van der Waals interactions, and switching was turned on using a switching distance of 8 Å and a pair list distance of 13.5 Å. Equations of motion were integrated every 2 fs. Finally, 5 ps simulations were run without constraints to complete the minimization and equilibration of the structures in the isothermal−isobaric ensemble at 300 K and 1 atm. Langevin dynamics were used to control the temperature with the dampening coefficient set to 5 ps^{-1}, and just applied to the heavy atoms. Periodic boundary conditions were applied and full-system periodic electrostatic interactions were calculated using the particle mesh Ewald method (*57*−*59*). A cutoff of 12 Å was set, and switching was turned on using a switching distance of 10 Å and a pair list distance of 13.5 Å. The final coordinates for each run were displayed and analyzed by VMD (*60*) and PROCHECK (*52*) and were superimposed by using the MOLMOL program (*61*).

RESULTS

Characterization of the Binding of an HPV E6 C-Terminal Peptide to the hDlg PDZ2 Domain. In an NMR titration experiment using ^{15}N-labeled-hDlg PDZ2 domain, the addition of a hexapeptide derived from the C-terminal sequence of HPV-18E6 (E6CT) induced substantial chemical shift changes in a subset of cross-peaks of the $^{1}H-^{15}N$ heteronuclear single quantum coherence (HSQC) spectrum (Figure 2A). Some peaks showed continuous changes in chemical shift as peptide was added (fast exchange), while some showed discontinuous changes with high intensity throughout the titration (slow exchange) or disappeared at the midpoint of the titration (intermediate exchange). As expected, large chemical shift changes were associated with peaks in slow chemical exchange, and small changes with peaks in fast exchange (Table S1, Supporting Information) (*34*, *62*). The chemical shift changes of residues in fast exchange (e.g., Gly327 and Lys351; Figure 2B and 2C) *versus* peptide concentration were fitted to eq 1 and generated an equilibrium dissociation constant of about 5.0 μM (Figure 1S, Supporting Information).

Table 1: Dissociation Constants (K_d) of the Binding between hDlg PDZ2 Domain and Hexapeptides[a]

peptide[b]	peptide/protein ratio	K_d (μM)	ΔH (kcal/mol)	$T\Delta S$ (kcal/mol)
E6CT	1.01 ± 0.02	1.33 ± 0.14	−10.1 ± 0.2	−2.0
E6CT0L	0.92 ± 0.02	6.49 ± 0.80	−8.3 ± 0.3	−1.3
E6CT4G	1.02 ± 0.10	5.18 ± 0.83	−7.1 ± 0.9	0.0
E6CT2p	n/a	n/a	n/a	n/a

[a] Isothermal titration calorimetry (ITC) experiments were run at 20 °C. Typically, a 200 μM peptide solution was injected into 10 μM PDZ2. "n/a" refers to a peptide which did not bind. [b] The peptides are E6CT, Ac-RRETQV-COOH; E6CT0L, Ac-RRETQL-COOH; E6CT2p, Ac-RRE_pTQV-COOH; E6CT4G, Ac-RGETQV-COOH.

The binding of the parent peptide and a series of mutant peptides to hDlg PDZ2 was also measured by isothermal titration calorimetry (ITC) (Table 1) and by NMR. All peptides that bound showed negative enthalpy changes (ΔH) varying from −7 to −10 kcal/mol, and small unfavorable entropy changes ($T\Delta S$) varying from 0 to −2 kcal/mol, indicating that binding is enthalpy-dominated. The wild-type HPV-18 E6 peptide, E6CT, yielded a dissociation constant of 1.3 ± 0.1 μM (corresponding to a ΔG value of −8.1 kcal/mol) with the predicted stoichiometry of 1.0:1.0 (Figure 2D). These results are consistent with those observed for other PDZ domain/target peptide interactions which have dissociation constants in the range of 1 to 10 μM (*63*, *64*). E6CT4G peptide, in which Arg154 was replaced by glycine, bound PDZ2 with a K_d value of 5.2 ± 0.8 μM (ΔG of −7.1 kcal/mol), which was around 4-fold weaker than E6CT. The energy contribution (ΔG) for binding PDZ2 from the side-chain contact made by Arg154 appears to be roughly 1 kcal/mol. E6CT0L peptide, in which the C-terminal valine

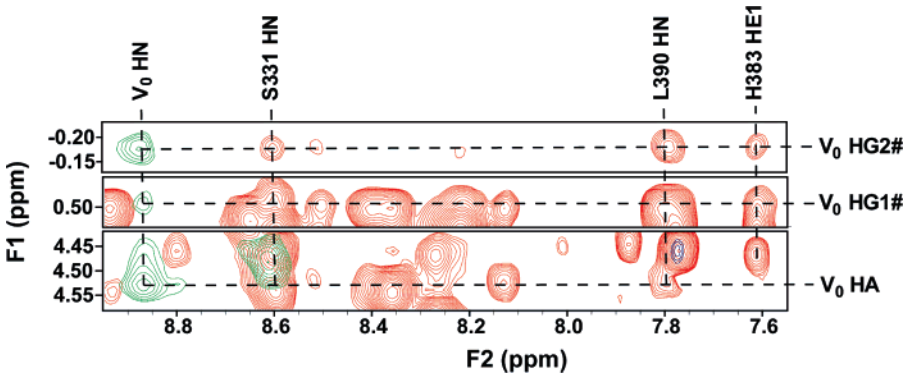

FIGURE 3: Determination of intermolecular NOEs between V_0 of E6CT and amides of the PDZ domain. The ^{13}C,^{15}N-filtered 2D NOESY (green contours) of ^{13}C,^{15}N-labeled hDlg PDZ2 domain in H_2O was superimposed with the 2D NOESY (red contours) and TOCSY (blue contours) of unlabeled hDlg PDZ2/E6CT at a ratio of 2:3 in D_2O.

was replaced by leucine, bound PDZ2 about 5-fold weaker than E6CT, with a dissociation constant of 6.5 ± 0.8 μM ($\Delta G = -7.0$ kcal/mol). The binding energy difference shows that valine at position 0 is about 1.1 kcal/mol more favorable for binding than leucine. E6CT2p, which was phosphorylated at Thr156, did not evolve heat on addition to PDZ2 in the ITC experiment, consistent with an inability to bind and indicating the crucial requirement of having unphosphorylated threonine at position −2 for interaction. To determine whether E6CT0L and E6CT4G bound to similar binding sites as E6CT, chemical shift changes were examined and found to be similar. The addition of E6CT2p yielded only small chemical shift changes at high peptide to PDZ domain ratios, indicating greatly reduced binding.

Three-Dimensional Structure of the hDlg PDZ2 Domain in Complex with the E6CT Peptide. We determined the 3D structure of the hDlg PDZ2 domain in complex with E6CT peptide using solution NMR spectroscopy. Samples containing ^{15}N-labeled or ^{15}N,^{13}C-labeled hDlg PDZ2 domain and unlabeled E6CT peptide were used for resonance and nuclear Overhauser effect (NOE) assignments. We carried out the backbone and side-chain assignments using standard methods (*41*, *42*). Except for the first residue (Met317), a residue located in a loop (Asn375), the three proline residues (Pro325, Pro341, and Pro404), and part of the His_6 tag, the backbone assignments were 100% completed. Except for Leu321, Leu371, and Val 373, whose two methyl groups could not be distinguished, the methyl groups from other six leucine residues and seven valine residues were stereospecifically assigned.

Using NOE cross-peaks from the 2D ^{15}N,^{13}C-filtered spectrum of ^{15}N,^{13}C-labeled hDlg PDZ2 in complex with unlabeled E6CT in H_2O as a basis set, intermolecular NOEs could be distinguished from intramolecular ones by comparing the spectra of overlaid 2D NOESY and TOCSY spectra of the unlabeled and unfiltered hDlg PDZ2/E6CT complex in D_2O (Figures 3 and S2, Supporting Information). This comparison was also used to analyze NOEs in the 3D ^{15}N-separated NOESY-HSQC. These data allowed us to assign 71 intermolecular NOEs between the E6CT peptide and the hDlg PDZ2 domain. Per residue, the numbers of intermolecular NOEs were 6 for residue R_{-5}, 3 for R_{-4}, 12 for E_{-3}, 10 for T_{-2}, 11 for Q_{-1} and 29 for V_0.

Structures of hDlg PDZ domain in complex with E6CT peptide were calculated using a final total of 1176 restraints (1126 NOEs and 25 hydrogen bonds), 163 dihedral restraints, and 87 $^1J_{NH}$ residual dipolar couplings. A ribbon diagram of a representative structure and a backbone superposition of 30 structures are shown in Figure 4. Over 98% of residues had favored phi−psi torsion angles by PROCHECK analysis (Table 2), and therefore the structure is of high quality. The total energies are about −203 kcal/mol, and the backbone rms deviation of superimposed structures is 0.46 ± 0.11 Å. To explore a greater range of motions than those exhibited by the NMR structures, simple molecular dynamic simulations were performed. The results with a variety of different molecular dynamic conditions showed that the conformations of residues V_0, Q_{-1}, and T_{-2} as well as the major structural elements of PDZ2 were the same as in the NMR structures (Figure S3, Supporting Information). Residues E_{-3}, R_{-4}, and R_{-5} in E6CT and loop 2 in PDZ2 showed alternative conformations, suggesting flexibility in the molecular contact between the N-terminal end of the peptide and the domain.

The solution structure of hDlg PDZ2 possesses a typical PDZ domain fold topology with six β-strands (βA to βF) and two α-helices (αA and αB) (Figure 4A) and is consistent with the crystal structures of the unliganded domain (*26*) and that bound to HPV-18 E6 peptide (*32*), with the rms deviation of the backbone atoms of superimposed secondary structure elements of about 0.9 Å. The difference is unlikely to be significant considering crystal packing artifacts and different crystallization conditions (*65*) and the uncertainty in the NMR coordinates (about 0.5 Å). The peptide docks to a positively charged groove between βB and αB, and forms a β strand (βG) that is antiparallel to βB.

The two methyl groups of the valine residue at the p0 position of E6CT are located in a hydrophobic pocket formed by the hydrophobic side chains of Leu328, Phe330, and Ile332 from the βB sheet and Ala386, Val387, Ala389, and Leu390 from the αB helix. The amide hydrogen of V_0 forms a hydrogen bond to the carbonyl O of Phe330, and one of the terminal carboxylates is recognized by hydrogen bonds to the HN from Leu328, Gly329, and Phe330 (Figure 4C). The two hydrophilic residues (glutamine at the p-1 position and threonine at the p-2 position) are in two shallow pockets and partly exposed to solvent, with two hydrogen bonds forming between T_{-2} and Ile332 (T_{-2}HN/Ile332O and T_{-2}O/Ile332HN). The negatively charged glutamate at the p-3 position is near a positive patch on the PDZ2 domain, and thus likely interacts with the PDZ2 domain through electrostatic interactions with His340 as well as a hydrogen bond suggested by NMR and MD simulations ($E_{-3}O\epsilon$/Thr350Hγ).

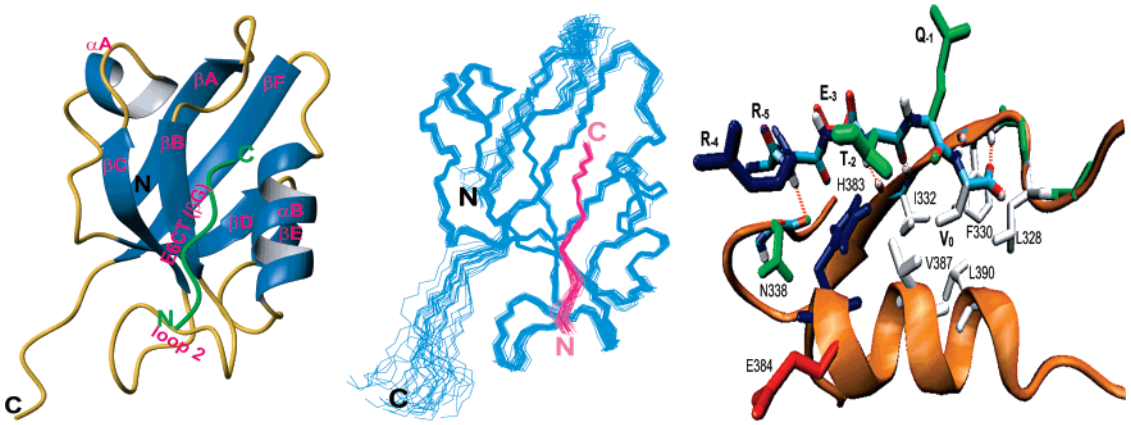

(A) (B) (C)

FIGURE 4: Structure and the interface of the hDlg PDZ2/E6CT complex. (A) Backbone structure of the complex. The α helices and the β sheet regions are in blue, connecting loops in yellow, and the E6CT peptide in green. Secondary elements are labeled sequentially from the N-terminus (N) to the C-terminus (C). (B) The thirty calculated structures of the hDlg PDZ2/E6CT complex. The structures were superimposed using the backbone atoms of residues in secondary structure elements of PDZ2 (βA, 318−322; βB, 330−333; βC, 347−352; αA, 357−361; βD, 369−373; βE, 376−377; αB, 383−391; βF 396−402) and the secondary structure element of E6CT (βG, E_{-3} to V_0). The N- and C-termini of the hDlg PDZ2 and E6CT are labeled. (C) The molecular interface between E6CT, labeled V_0 through R_{-5}, and PDZ2. Amino acid side chains of βB and αB of PDZ2 that participate in binding E6CT are shown and labeled.

Table 2: Structural Statistics for the hDlg PDZ2 Domain/E6CT Peptide Complex

Average Rms Deviations from Experimental Restraints		
NOE distance restraints (Å)	no.	deviation
all	1126	0.0186 ± 0.0009
intraresidual ($i = j$)	457	
sequential ($\|i - j\| = 1$)	260	
short range ($2 \leq \|i - j\| \leq 4$)	80	
long range ($\|i - j\| \geq 5$)	258	
intermolecular	71	
hydrogen bond	25	
dihedral restraints	163	
RDC	87	

Rms Deviations from Ideal Stereochemistry	
bonds (Å)	0.0032 ± 0.0001
angles (deg)	0.4959 ± 0.0121
impropers (deg)	0.4478 ± 0.0216

Ramachandran Analysis[a]	
residues in favored regions	86.1%
residues in additionally allowed regions	12.7%
residues in generously allowed regions	1.3%
residues in disallowed regions	0.0%

Average Rms Deviations from Atomic Coordinates (Å)	
backbone (Å)[b]	0.46 ± 0.11
heavy atoms (Å)[b]	0.97 ± 0.13

[a] Calculated with PROCHECK. [b] 30 structures were superimposed using the backbone atoms of residues in secondary structure elements of PDZ2 (319−323, 331−334, 348−353, 358−362, 370−374, 377−378, 384−392, 397−403) and E_{-3} to V_0 of E6CT. The corresponding secondary structures are βA, βB, βC, αA, βD, βE, αB, βF in PDZ2 and βG in the peptide ligand.

Arginine at the p-4 position forms hydrogen bonds with Asn338 and Gly334 (R_{-4}HN/Asn338O and R_{-4}O/Asn338Hδ and R_{-4}O/Gly334HN). MD simulations suggest an interaction between the side chain Hϵ of R_{-4} and the side chain Oδ of Asn338. Although this arginine is near a positively charged area of the PDZ2 domain, intermolecular NOEs between R_{-4} and His383 indicated that the relatively poorly defined side chain of R_{-4} extends toward Glu384, potentially forming a salt bridge which would lessen an otherwise disadvantageous electrostatic interaction. Thus Gly334 and Asn338 within loop 2 and Glu384 in αB are important for R_{-4} binding. The arginine at the p-5 position extends away from the PDZ2 domain, and avoids a potentially disadvantageous electrostatic interaction associated with the positively charged surface of the peptide-binding region of the domain. MD simulations showed a potential hydrogen bond between the side chain of R_{-5}(Hη11) and His340Nδ, consistent with NOEs observed by NMR. The residues in loop 2 (Gly334, Asn338, and His340) of PDZ2 thus form a binding motif for R_{-5}, R_{-4}, and E_{-3} of E6CT that has not been previously reported for other PDZ domains.

The chemical shift perturbations of PDZ2 residues on binding E6CT were examined in detail to refine the binding model suggested by the structure. The residues displaying large chemical shift changes ($\Delta > 0.15$ ppm) mapped to one face of the domain structure (Figure 5). Generally, the buried residues contacting the peptide displayed large chemical shift changes and slow exchange rates. These include Leu328, Gly329, Ala389, and Leu390 of the hydrophobic pocket of PDZ2 that are close to V_0 in E6CT and residues Thr350, His383, and Ile353 that are close to residues E_{-3}, T_{-2}, and Q_{-1}, respectively. The residues not participating in binding and exposed to solvent displayed either small or no chemical shift changes and fast exchange rates. The residues possessing strong contacts to the peptide but exposed to solvent displayed medium chemical shift changes and intermediate exchange rates. The NMR chemical shift changes for residues showing fast exchange at the periphery of the binding site (residues Gly327, Lys351, Thr393, and Phe396) were suitable for analysis, and yielded an average equilibrium dissociation constant (K_d) of ~5 μM. These residues, which do not directly contact the bound E6CT peptide, appeared to show weaker binding affinities than that measured globally using isothermal titration calorimetry ($K_d \sim 1$ μM). The difference may not be significant, reflecting the different protein concentrations used in the two experiments, but may also indicate a multistate binding phenomenon in which the residues directly contacting the bound E6CT peptide bind

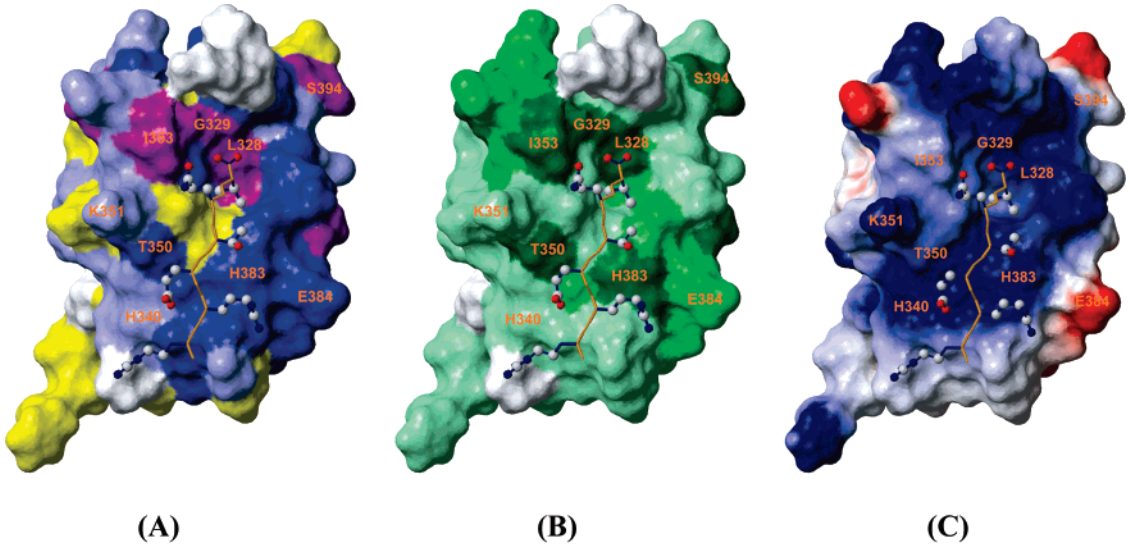

FIGURE 5: Mapping of chemical shift changes in the hDlg PDZ2 domain on binding E6CT peptide and its electrostatic potential surface. The hDlg PDZ2 domain is shown as a surface whereas for E6CT the side-chain atoms are shown in ball and stick and the backbone atoms are shown as an orange line. Residues of PDZ2 that directly contact the peptide and otherwise participate in binding are labeled. (A) Chemical shift changes are mapped onto the structure of the complex. Color coding is based on the magnitude of chemical shift perturbation ($\Delta = [(\Delta\delta HN)^2 + (0.11\Delta\delta N)^2]^{1/2}$): white, no data available; yellow, no change ($\Delta < 0.05$ ppm); light blue, small change ($0.05 \leq \Delta < 0.10$ ppm); blue, medium change ($0.10 \leq \Delta < 0.15$ ppm); purple, large change ($\Delta \geq 0.15$ ppm). (B) Chemical shift exchange rates of amides upon titration. Residues with fast exchange (including residues that do not shift significantly on binding peptide) are shown in light green; those with intermediate exchange are in mid-green; those with slow exchange are shown in dark green; those which could not be determined are in white. (C) Electrostatic potential surface of hDlg PDZ2 as calculated by MOLMOL (*61*). Positive potential is shown in blue, and negative potential is in red.

with higher affinity, consistent with previous observations of SH2 binding to phosphotyrosine-containing peptides (*66*).

DISCUSSION

Comparison of Closely Related PDZ Domain Structures Binding to Different Peptides. The crystal structure of the second PDZ domain of hDlg alone and in complex with a peptide from the C-terminus of GluR-A (Ala_{904}-Thr_{905}-Gly_{906}-Leu_{907}) was recently determined (*26*). Because the complex is a dimer showing two PDZ domains in the asymmetric unit with different resolution, the chain with best resolution (chain A) was selected for analysis. To examine the conformation changes in hDlg PDZ2 that occur in the βB and αB secondary elements that are in closest contact to the peptide, the other secondary structural elements (βA, βC − βF, and αA) were superimposed (Figure 6). Although the overall structures are similar (rms deviation of superimposed backbone atoms of ~1 Å), significant differences appear to arise from ligand-induced conformational changes. The changes may arise from crystal packing forces which can induce up to 1 Å changes in loop conformations (*65*). In particular, in the PDZ2/GluR-A complex (and in the crystal structure of the PDZ2/E6CT complex), crystal contacts were found to involve loop 2. In the PDZ2/GluR-A complex, the C-terminus of αB moves away from the βB sheet, consistent with an interpretation that the movement facilitates accommodation of the peptide (*26*, *67*), whereas in the PDZ2/E6CT complex, the C-terminus of αB is closer to βB, making the structure more compact. Conformational differences may arise from differences in the size of the p0 residue which is leucine in PDZ2/GluR-A and the smaller valine in PDZ2/E6CT. Examination of the potential surfaces shows that the hydrophobic pocket that surrounds valine in PDZ2/E6CT is smaller than the corresponding pockets in PDZ2/GluR-A and

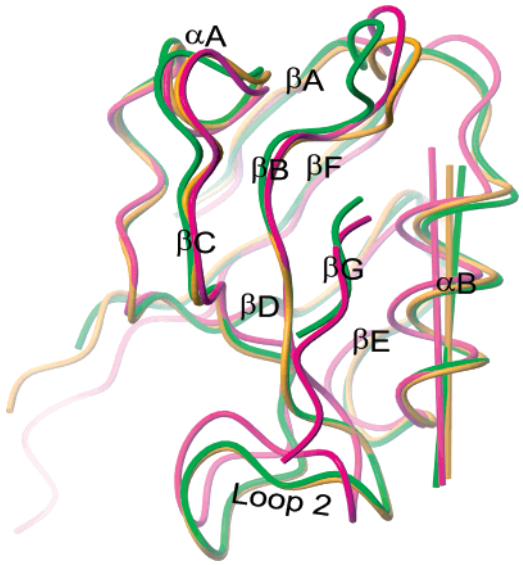

FIGURE 6: Bound and unbound hDlg PDZ2 domain. The backbones are shown for the hDlg PDZ2/E6CT complex (magenta); the hDlg PDZ2/GluR-A complex (green); and unliganded hDlg PDZ2 (orange). To compare changes in the secondary elements that contact the peptide ligand (βB and αB), backbone atoms were superimposed using the remaining secondary structural elements and loops. The secondary structural elements and loop 2 are labeled. The axis of the principal helix involved in binding is shown as a bar with the corresponding colors for each structure.

PDZ2 alone. Differences in the center of the distance difference matrix (DDM) confirm that the core structure of PDZ2/E6CT is more compact than PDZ2/GluR-A (Figure S4, Supporting Information). The suitability of valine over leucine at the p0 position suggested by the structures is consistent with the ITC measurements showing stronger binding to the valine-containing peptide (Table 1). Such structural and energetic comparisons explain the higher

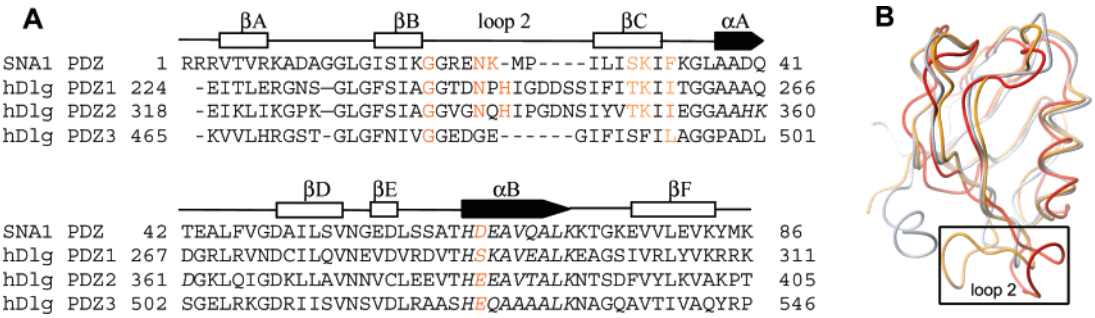

FIGURE 7: Sequences and structures of the three hDlg PDZ domains and the SNA1 PDZ domain. (A) Alignment of the three hDlg PDZ domain sequences and that of SNA1. The critical residues proposed to participate in residue-specific binding are highlighted, and the secondary structure elements are shown above the sequence: loops are in solid line, sheets in open rectangles, and helices in filled pentagons. Residues participating in binding are in orange. (B) Backbone superimposition of the three unliganded hDlg PDZ domains, from PDB entries 1ZOK, 2AWX, and 1PDR, respectively. PDZ1 (red); PDZ2 (orange); PDZ3 (gray) are superimposed using secondary structures. The different conformations of loop 2 are highlighted by a box.

affinity of HPV-18 E6 over HPV-16 E6 for binding hDlg PDZ2, which had been demonstrated qualitatively by GST-pulldown assays (*12*). The only difference in their PDZ-binding motifs is the p0 residue, which is leucine in HPV-16 E6 and valine in HPV-18 E6.

The crystal structure of hDlg PDZ2/GluR-A showed that βB of PDZ2 interacts at positions p0 and p-2 of the bound peptide through main chain hydrogen bonds, consistent with a "classical" type I PDZ interaction (*20*, *26*, *63*, *64*). The high-risk HPV E6 proteins contain not only the highly conserved E_{-3}-T_{-2}-Q_{-1}-V_0 sequence but also two additionally conserved arginine residues at the p-4 and p-5 positions. As a consequence of more extensive engagement of residues of PDZ2 in contacting E6CT than when contacting GluR-A, differences in conformation arise, resulting in an rms deviation of superimposed backbone atoms of 1.7 Å. In PDZ2/E6CT, there is van der Waals contact between Q_{-1} and Ile353 (Figure 5), which is absent in PDZ2/GluR-A. The hydrogen bond between R_{-4}HN and Asn338O in PDZ2/E6CT is absent in PDZ2/GluR-A. Another major difference between PDZ2/E6CT and PDZ2/GluR-A is in loop 2, which is more packed and closer to the C-terminus of the βB sheet in the PDZ2/E6CT complex than in PDZ2/GluR-A (*26*).

The additional contacts observed in the hDlg PDZ2/E6CT complex may provide the driving force for the more compact nature of its structure and the more rigid conformation of its loop 2 than in the other PDZ domains. A large number of NOEs between His383 in the first position of helix αB and residues Ile332/Ala333/Gly334 in the βB strand and Asn338 in loop 2 demonstrate significant interaction between the N-terminus of αB and the C-terminus of βB/loop2. In the unliganded hDlg PDZ2 crystal structure, four hydrogen bonds were observed involving loop 2 (Asn338 HN/Gly335O, Asp344 HN/Ile341O, Gly343HN/Gln339Oϵ1, and Ser346HN/Asp344Oδ1). In the PDZ2/GluR-A complex, three additional hydrogen bonds (Gly334HN/Asn338O, Asn338Hδ21/Gly334O, and Asn339Hϵ21/Asn345Oδ1, respectively) are generated. In the PDZ2/E6CT complex, two more hydrogen bonds are present, Gly335HN/Asn345O and one between αB and loop 2 through His383Hδ1/Gly334O. The extensive contacts of R_{-4} and R_{-5} in E6CT with loop 2 appear to slide the peptide in the groove between βB and αB toward loop 2. Consequently, the contacts made from loop 2 to His383 in αB pull the C-terminus of the helix to reorient inside and make the PDZ2 domain more compact.

Comparison of Different PDZ Domain Structures Binding to Similar Target Peptide Sequences. The PDZ domain of SNA1 (α-1-syntrophin) recognizes five C-terminal residues of the α-subunit of the vertebrate voltage-gated sodium channel with a hydrophobic residue at p0, a S/T residue at p-2, an E at p-3, and R/K at p-4 with a dissociation constant of 2.1 μM (*64*, *68*). The similarity of its recognition sequence to the extended C-terminal recognition sequences in high-risk HPV E6 proteins and the comparable binding affinities suggests similar molecular interactions. Comparison of the hDlg PDZ2/E6CT structure with the NMR structure of the PDZ domain of SNA1 in complex with a peptide G_{-6}-V_{-5}-K_{-4}-E_{-3}-S_{-2}-L_{-1}-V_0 (*68*) shows that the residues interacting with V_0 are very similar in terms of van der Waals contacts and hydrogen bonds. In PDZ2/E6CT, Ile353 is in van der Waals contact with Q_{-1}, whereas in the SNA1 PDZ complex, the equivalent residue is Phe34, which contacts L_{-1}. The hDlg PDZ2 Ile332 contacts T_{-2} of E6CT through two main-chain hydrogen bonds (T_{-2}O/Ile332HN and T_{-2}HN/Ile332O); the corresponding contacts in the SNA1-PDZ complex are S_{-2}HN/Ile18O and potentially S_{-2}OH/His64Nϵ. Similar interactions are also made in both complexes in contacting the glutamate residue at the p-3 position.

SNA1 PDZ and hDlg PDZ2 differ in their contacts to residues in the p-4 and p-5 position of the peptide. Although both contact arginine (or lysine) at the p-4 position, specificity is provided by different residues, mostly as a consequence of loop 2 being five amino acids shorter in SNA1-PDZ. Three key residues of hDlg PDZ2 are used to select arginine at the p-4 position (Gly334 and Asn338 of loop2 and Glu384 of αB). The Asp65 of SNA1-PDZ, which is equivalent to Glu384 in hDlg PDZ2, is the only contact to provide specificity for the p-4 position. In SNA1-PDZ, Gly20 (the equivalent of Gly334) contacts a histidine in αB within the domain, whereas in hDlg PDZ2 the residue hydrogen bonds with Asn338 within loop 2 that contacts R_{-4}. Asn24 in SNA1 PDZ, equivalent to Asn338 in hDlg PDZ2, is too far away to interact with K_{-4}. The hDlg PDZ2 domain shows specificity for arginine at the −5 position using His340, whereas SNA1 PDZ does not have residues in loop 2 that could carry out similar interactions, and therefore it does not show specificity at the −5 position.

Because the syntrophin SNA1 PDZ domain binds to a sequence that is at the C-terminus of HPV E6 proteins, we predict that HPV E6 targets syntrophin SNA1 in addition to

the seven PDZ domain-containing proteins that have been reported (*69*). Syntrophins are scaffold proteins of the dystrophin glycoprotein complex that targets ion channels, receptors, and signaling proteins to specialized subcellular domains (*70*). The PDZ domain of syntrophins serves as an adaptor for recruiting membrane channels, receptors, kinases, and other signaling proteins (*71*). It is possible then that HPV E6 affects the biological functions of SNA1.

hDlg PDZ2 Binds E6 with Highest Affinity Compared to hDlg PDZ1 and PDZ3. The structures of the three PDZ domains of hDlg have been determined in the unliganded state (*18*, *26*, *27*), the solution structure of hDlg PDZ2 in complex with E6CT is described in the present work, and the structures of the domains in complex with a peptide similar to E6CT have been solved using X-ray crystallography (*32*). These structures allow us to provide a molecular explanation for why hDlg PDZ2 has been found to be a good domain for binding HPV E6 compared to the hDlg PDZ1 and PDZ3 domains (*5*, *6*, *18*, *19*). The sequences of the three PDZ domains are shown in Figure 7. Gly334, Asn338, and His340 in loop 2 and Glu384 in αB of PDZ2 make contact to E6CT at R_{-4} and R_{-5}, whereas in PDZ1, the corresponding residues are Gly, Asn, His, and Ser. Most of the critical residues of hDlg PDZ2 needed for binding R_{-4} and R_{-5} are also present in PDZ1, suggesting that PDZ1 could bind to E6CT in a similar manner. Because the side chain of Ser290 in PDZ1 is neutral and short, it cannot contact R_{-4} in the same manner as the long, negatively charged side chain of Glu384 in PDZ2. However, residues in loop 2 and a threonine and lysine in βC are in the correct position to contact E_{-3}, thus allowing PDZ1 to still bind HPV E6. In addition, instead of a glutamine at residue 339 in PDZ2, the corresponding residue in PDZ1 is proline (residue 245), which sits between the two key residues, Asn244 and His246, that potentially contact the arginines at p-4 and p-5. It appears that the presence of proline in the loop distorts the conformation and reduces the binding of PDZ1 to HPV E6 protein relative to PDZ2. In a study that examined binding to the protein NR2B, mutation of this proline to glutamine led to a 2-fold increase in affinity (*18*). In PDZ3, the residues corresponding to loop 2 of PDZ2 are 6 amino acids shorter, and therefore it does not contain the crucial residues for the contacts to R_{-4} and R_{-5} residues, thus explaining its greatly decreased ability to bind E6. Analysis of the crystal structures suggests an alternative model for weak PDZ3 binding in which Leu494 and Asn478 sterically prevent contact to Q_{-1} (*32*). Although in SNA1 PDZ, hDlg PDZ1, and PDZ2 domains, the residues corresponding to Leu494 in PDZ3 are the equally large Phe or Ile residues (Figure 7), they still bind peptide targets with high affinity. Mutational analysis of E6 peptides and PDZ3 domains could be used to investigate the relative contributions of changes in contacts to the −1 position of bound peptide versus a model which invokes changes in contacts to the −4 and −5 positions.

Interestingly, high-risk HPV E6 binds both the central, DNA-binding domain of p53 (*72*) and hDlg (*73*). We speculate that the hDlg−E6−E6AP triple complex has features similar to the p53−E6−E6AP complex as they both experience ubiquitin-mediated degradation processes. The part of E6 that binds E6AP (or another ubiquitin ligase) possibly possesses the same molecular surface in both hDlg−E6 and p53−E6 complexes. Thus this structure investigation of HPV E6 with hDlg provides a model to understand the binding and subsequent degradation of both p53 and PDZ-containing target proteins.

ACKNOWLEDGMENT

We thank Dr. James Sudmeier and Jie Wei for help with setting up 3D NMR experiments.

SUPPORTING INFORMATION AVAILABLE

One table summarizing chemical shift perturbations and exchange of hDlg PDZ2 domain upon peptide titration, and four figures showing NMR data fitting, intermolecular NOEs, comparison of solution structures, and MD results. This material is available free of charge via the Internet at http://pubs.acs.org.

REFERENCES

1. Munoz, N., Bosch, F. X., de Sanjose, S., Herrero, R., Castellsague, X., Shah, K. V., Snijders, P. J., and Meijer, C. J. (2003) Epidemiologic classification of human papillomavirus types associated with cervical cancer, *N. Engl. J. Med. 348*, 518−527.
2. Clifford, G. M., Smith, J. S., Plummer, M., Munoz, N., and Franceschi, S. (2003) Human papillomavirus types in invasive cervical cancer worldwide: a meta-analysis, *Br. J. Cancer 88*, 63−73.
3. Franco, E. L., Schlecht, N. F., and Saslow, D. (2003) The epidemiology of cervical cancer, *Cancer J. 9*, 348−359.
4. Thomas, M., Pim, D., and Banks, L. (1999) The role of the E6−p53 interaction in the molecular pathogenesis of HPV, *Oncogene 18*, 7690−7700.
5. Kiyono, T., Hiraiwa, A., Fujita, M., Hayashi, Y., Akiyama, T., and Ishibashi, M. (1997) Binding of high-risk human papillomavirus E6 oncoproteins to the human homologue of the Drosophila discs large tumor suppressor protein, *Proc. Natl. Acad. Sci. U.S.A. 94*, 11612−11616.
6. Lee, S. S., Weiss, R. S., and Javier, R. T. (1997) Binding of human virus oncoproteins to hDlg/SAP97, a mammalian homolog of the Drosophila discs large tumor suppressor protein, *Proc. Natl. Acad. Sci. U.S.A. 94*, 6670−6675.
7. Nakagawa, S., and Huibregtse, J. M. (2000) Human scribble (Vartul) is targeted for ubiquitin-mediated degradation by the high-risk papillomavirus E6 proteins and the E6AP ubiquitin-protein ligase, *Mol. Cell Biol. 20*, 8244−8253.
8. Lee, S. S., Glaunsinger, B., Mantovani, F., Banks, L., and Javier, R. T. (2000) Multi-PDZ domain protein MUPP1 is a cellular target for both adenovirus E4-ORF1 and high-risk papillomavirus type 18 E6 oncoproteins, *J. Virol. 74*, 9680−9693.
9. Glaunsinger, B. A., Lee, S. S., Thomas, M., Banks, L., and Javier, R. (2000) Interactions of the PDZ-protein MAGI-1 with adenovirus E4-ORF1 and high-risk papillomavirus E6 oncoproteins, *Oncogene 19*, 5270−5280.
10. Thomas, M., Laura, R., Hepner, K., Guccione, E., Sawyers, C., Lasky, L., and Banks, L. (2002) Oncogenic human papillomavirus E6 proteins target the MAGI-2 and MAGI-3 proteins for degradation, *Oncogene 21*, 5088−5096.
11. Scheffner, M., Huibregtse, J. M., Vierstra, R. D., and Howley, P. M. (1993) The HPV-16 E6 and E6-AP complex functions as a ubiquitin-protein ligase in the ubiquitination of p53, *Cell 75*, 495−505.
12. Pim, D., Thomas, M., Javier, R., Gardiol, D., and Banks, L. (2000) HPV E6 targeted degradation of the discs large protein: evidence for the involvement of a novel ubiquitin ligase, *Oncogene 19*, 719−725.
13. Gardiol, D., Kuhne, C., Glaunsinger, B., Lee, S. S., Javier, R., and Banks, L. (1999) Oncogenic human papillomavirus E6 proteins target the discs large tumour suppressor for proteasome-mediated degradation, *Oncogene 18*, 5487−5496.
14. Massimi, P., Gammoh, N., Thomas, M., and Banks, L. (2004) HPV E6 specifically targets different cellular pools of its PDZ domain-containing tumour suppressor substrates for proteasome-mediated degradation, *Oncogene 23*, 8033−8039.
15. Matsumoto, Y., Nakagawa, S., Yano, T., Takizawa, S., Nagasaka, K., Nakagawa, K., Minaguchi, T., Wada, O., Ooshi, H., Matsu-

moto, K., Yasugi, T., Kanda, T., Huibregtse, J. M., and Taketani, Y. (2006) Involvement of a cellular ubiquitin-protein ligase E6AP in the ubiquitin-mediated degradation of extensive substrates of high-risk human papillomavirus E6, *J. Med. Virol. 78*, 501−507.
16. Suzuki, T., Ohsugi, Y., Uchida-Toita, M., Akiyama, T., and Yoshida, M. (1999) Tax oncoprotein of HTLV-1 binds to the human homologue of Drosophila discs large tumor suppressor protein, hDLG, and perturbs its function in cell growth control, *Oncogene 18*, 5967−5972.
17. Matsumine, A., Ogai, A., Senda, T., Okumura, N., Satoh, K., Baeg, G. H., Kawahara, T., Kobayashi, S., Okada, M., Toyoshima, K., and Akiyama, T. (1996) Binding of APC to the human homolog of the Drosophila discs large tumor suppressor protein, *Science 272*, 1020−1023.
18. Wang, L., Piserchio, A., and Mierke, D. F. (2005) Structural characterization of the intermolecular interactions of synapse-associated protein-97 with the NR2B subunit of N-methyl-D-aspartate receptors, *J. Biol. Chem. 280*, 26992−26996.
19. Gaudet, S., Branton, D., and Lue, R. A. (2000) Characterization of PDZ-binding kinase, a mitotic kinase, *Proc. Natl. Acad. Sci. U.S.A. 97*, 5167−5172.
20. Kang, B. S., Cooper, D. R., Devedjiev, Y., Derewenda, U., and Derewenda, Z. S. (2003) Molecular roots of degenerate specificity in syntenin's PDZ2 domain: reassessment of the PDZ recognition paradigm, *Structure 11*, 845−853.
21. Lee, C., and Laimins, L. A. (2004) Role of the PDZ domain-binding motif of the oncoprotein E6 in the pathogenesis of human papillomavirus type 31, *J. Virol. 78*, 12366−12377.
22. Simonson, S. J., Difilippantonio, M. J., and Lambert, P. F. (2005) Two distinct activities contribute to human papillomavirus 16 E6's oncogenic potential, *Cancer Res. 65*, 8266−8273.
23. Ishidate, T., Matsumine, A., Toyoshima, K., and Akiyama, T. (2000) The APC-hDLG complex negatively regulates cell cycle progression from the G0/G1 to S phase, *Oncogene 19*, 365−372.
24. Kuhne, C., Gardiol, D., Guarnaccia, C., Amenitsch, H., and Banks, L. (2000) Differential regulation of human papillomavirus E6 by protein kinase A: conditional degradation of human discs large protein by oncogenic E6, *Oncogene 19*, 5884−5891.
25. Watson, R. A., Thomas, M., Banks, L., and Roberts, S. (2003) Activity of the human papillomavirus E6 PDZ-binding motif correlates with an enhanced morphological transformation of immortalized human keratinocytes, *J. Cell Sci. 116*, 4925−4934.
26. von Ossowski, I., Oksanen, E., von Ossowski, L., Cai, C., Sundberg, M., Goldman, A., and Keinanen, K. (2006) Crystal structure of the second PDZ domain of SAP97 in complex with a GluR-A C-terminal peptide, *FEBS J. 273*, 5219−5229.
27. Morais, Cabral, J. H., Petosa, C., Sutcliffe, M. J., Raza, S., Byron, O., Poy, F., Marfatia, S. M., Chishti, A. H., and Liddington, R. C. (1996) Crystal structure of a PDZ domain, *Nature 382*, 649−652.
28. Tochio, H., Hung, F., Li, M., Bredt, D. S., and Zhang, M. (2000) Solution structure and backbone dynamics of the second PDZ domain of postsynaptic density-95, *J. Mol. Biol. 295*, 225−237.
29. Doyle, D. A., Lee, A., Lewis, J., Kim, E., Sheng, M., and MacKinnon, R. (1996) Crystal structures of a complexed and peptide-free membrane protein-binding domain: molecular basis of peptide recognition by PDZ, *Cell 85*, 1067−1076.
30. Hillier, B. J., Christopherson, K. S., Prehoda, K. E., Bredt, D. S., and Lim, W. A. (1999) Unexpected modes of PDZ domain scaffolding revealed by structure of nNOS-syntrophin complex, *Science 284*, 812−815.
31. Tochio, H., Zhang, Q., Mandal, P., Li, M., and Zhang, M. (1999) Solution structure of the extended neuronal nitric oxide synthase PDZ domain complexed with an associated peptide, *Nat. Struct. Biol. 6*, 417−421.
32. Zhang, Y., Dasgupta, J., Ma, R. Z., Banks, L., Thomas, M., and Chen, X. S. (2007) Structures of a HPV-E6 polypeptide bound to MAGUK proteins: mechanisms of targeting tumor suppressors by a high-risk HPV oncoprotein, *J. Virol. 87*, 3618−3626.
33. Reilly, D., and Fairbrother, W. J. (1994) A novel isotope labeling protocol for bacterially expressed proteins, *J. Biomol. NMR 4*, 459−462.
34. Kim, S., Cullis, D. N., Feig, L. A., and Baleja, J. D. (2001) Solution structure of the Reps1 EH domain and characterization of its binding to NPF target sequences, *Biochemistry 40*, 6776−6785.
35. Lu, J., Li, H., Wang, Y., Sudhof, T. C., and Rizo, J. (2005) Solution structure of the RIM1alpha PDZ domain in complex with an ELKS1b C-terminal peptide, *J. Mol. Biol. 352*, 455−466.
36. Garcia, J., Gerber, S. H., Sugita, S., Sudhof, T. C., and Rizo, J. (2004) A conformational switch in the Piccolo C2A domain regulated by alternative splicing, *Nat. Struct. Mol. Biol. 11*, 45−53.
37. Kay, L. E., Xu, G. Y., Singer, A. U., Muhandiram, D. R., and Formankay, J. D. (1993) A gradient-enhanced HCCH-TOCSY experiment for recording side-chain 1H and 13C correlations in H2O samples of proteins, *J. Magn. Reson. B 101*, 333−337.
38. Kay, L. E., Xu, G. Y., and Yamazaki, T. (1994) Enhanced-sensitivity triple-resonance spectroscopy with minimal H2O saturation, *J. Magn. Reson. A 109*, 129−133.
39. Muhandiram, D. R., and Kay, L. E. (1994) Gradient-enhanced triple-resonance 3-dimensional NMR experiments with improved sensitivity, *J. Magn. Reson. B 103*, 203−216.
40. Zhang, O. W., Kay, L. E., Olivier, J. P., and Formankay, J. D. (1994) Backbone H-1 and N-15 resonance assignments of the N-terminal SH3 domain of drk in folded and unfolded states using enhanced-sensitivity pulsed-field gradient NMR techniques, *J. Biomol. NMR 4*, 845−858.
41. Sattler, M., Schleucher, J., and Griesinger, C. (1999) Heteronuclear multidimensional NMR experiments for the structure determination of proteins in solution employing pulsed field gradients, *Prog. Nucl. Magn. Reson. Spectrosc. 34*, 93−158.
42. Clore, G. M., and Gronenborn, A. M. (1998) Determining the structures of large proteins and protein complexes by NMR, *Trends Biotechnol. 16*, 22−34.
43. Ruckert, M., and Otting, G. (2000) Alignment of biological macromolecules in novel nonionic liquid crystalline media for NMR experiments, *J. Am. Chem. Soc. 122*, 7793−7797.
44. Neri, D., Szyperski, T., Otting, G., Senn, H., and Wuthrich, K. (1989) Stereospecific nuclear magnetic resonance assignments of the methyl groups of valine and leucine in the DNA-binding domain of the 434 repressor by biosynthetically directed fractional 13C labeling, *Biochemistry 28*, 7510−7516.
45. Neri, D., Otting, G., and Wuthrich, K. (1990) H-1 and C-13 NMR chemical-shifts of the diastereotopic methyl-groups of valyl and leucyl residues in peptides and proteins, *Tetrahedron 46*, 3287−3296.
46. Vuister, G. W., Kim, S. J., Wu, C., and Bax, A. (1994) 2D and 3D NMR-study of phenylalanine residues in proteins by reverse isotopic labeling, *J. Am. Chem. Soc. 116*, 9206−9210.
47. Goddard, T. D., and Kneller, D. G., SPARKY 3, University of California, San Francisco
48. Cornilescu, G., Delaglio, F., and Bax, A. (1999) Protein backbone angle restraints from searching a database for chemical shift and sequence homology, *J. Biomol. NMR 13*, 289−302.
49. Brunger, A. T., Adams, P. D., Clore, G. M., DeLano, W. L., Gros, P., Grosse-Kunstleve, R. W., Jiang, J. S., Kuszewski, J., Nilges, M., Pannu, N. S., Read, R. J., Rice, L. M., Simonson, T., and Warren, G. L. (1998) Crystallography & NMR system: A new software suite for macromolecular structure determination, *Acta Crystallogr., Sect. D: Biol. Crystallogr. 54*, 905−921.
50. Liu, Y., Liu, Z., Androphy, E., Chen, J., and Baleja, J. D. (2004) Design and characterization of helical peptides that inhibit the E6 protein of papillomavirus, *Biochemistry 43*, 7421−7431.
51. Zweckstetter, M., and Bax, A. (2000) Prediction of sterically induced alignment in a dilute liquid crystalline phase: aid to protein structure determination by NMR, *J. Am. Chem. Soc. 122*, 3791−3792.
52. Laskowski, R. A., MacArthur, M. W., Moss, D. S., and Thornton, J. M. (1993) Procheck—a program to check the stereochemical quality of protein structures, *J. Appl. Crystallogr. 26*, 283−291.
53. Vriend, G. (1990) What If—a molecular modeling and drug design program, *J. Mol. Graphics 8*, 52−56.
54. Schneider, T. R. (2002) A genetic algorithm for the identification of conformationally invariant regions in protein molecules, *Acta Crystallogr., Sect. D: Biol. Crystallogr. 58*, 195−208.
55. Phillips, J. C., Braun, R., Wang, W., Gumbart, J., Tajkhorshid, E., Villa, E., Chipot, C., Skeel, R. D., Kale, L., and Schulten, K. (2005) Scalable molecular dynamics with NAMD, *J. Comput. Chem. 26*, 1781−1802.
56. MacKerell, A. D., Bashford, D., Bellott, M., Dunbrack, R. L., Evanseck, J. D., Field, M. J., Fischer, S., Gao, J., Guo, H., Ha, S., Joseph-McCarthy, D., Kuchnir, L., Kuczera, K., Lau, F. T. K., Mattos, C., Michnick, S., Ngo, T., Nguyen, D. T., Prodhom, B., Reiher, W. E., Roux, B., Schlenkrich, M., Smith, J. C., Stote, R., Straub, J., Watanabe, M., Wiorkiewicz-Kuczera, J., Yin, D.,

and Karplus, M. (1998) All-atom empirical potential for molecular modeling and dynamics studies of proteins, *J. Phys. Chem. B 102*, 3586−3616.
57. Darden, T., York, D., and Pedersen, L. (1993) Particle Mesh Ewald−an N.Log(N) method for Ewald sums in large systems, *J. Chem. Phys. 98*, 10089−10092.
58. York, D. M., Darden, T. A., and Pedersen, L. G. (1993) The effect of long-range electrostatic interactions in simulations of macromolecular crystals−a comparison of the Ewald and truncated list methods, *J. Chem. Phys. 99*, 8345−8348.
59. York, D. M., Wlodawer, A., Pedersen, L. G., and Darden, T. A. (1994) Atomic-level accuracy in simulations of large protein crystals, *Proc. Natl. Acad. Sci. U.S.A. 91*, 8715−8718.
60. Humphrey, W., Dalke, A., and Schulten, K. (1996) VMD: visual molecular dynamics, *J. Mol. Graphics 14*, 33−38.
61. Koradi, R., Billeter, M., and Wuthrich, K. (1996) MOLMOL: a program for display and analysis of macromolecular structures, *J. Mol. Graphics 14*, 51−32.
62. Feeney, J., Batchelor, J. G., Albrand, J. P., and Roberts, G. C. K. (1979) Effects of intermediate exchange processes on the estimation of equilibrium-constants by NMR, *J. Magn. Reson. 33*, 519−529.
63. Nourry, C., Grant, S. G., and Borg, J. P. (2003) PDZ domain proteins: plug and play!, *Sci. STKE. 2003*, RE7.
64. Wiedemann, U., Boisguerin, P., Leben, R., Leitner, D., Krause, G., Moelling, K., Volkmer-Engert, R., and Oschkinat, H. (2004) Quantification of PDZ domain specificity, prediction of ligand affinity and rational design of super-binding peptides, *J. Mol. Biol. 343*, 703−718.
65. Eyal, E., Gerzon, S., Potapov, V., Edelman, M., and Sobolev, V. (2005) The limit of accuracy of protein modeling: influence of crystal packing on protein structure, *J. Mol. Biol. 351*, 431−442.
66. Gunther, U., Mittag, T., and Schaffhausen, B. (2002) Probing Src homology 2 domain ligand interactions by differential line broadening, *Biochemistry 41*, 11658−11669.
67. Grembecka, J., Cierpicki, T., Devedjiev, Y., Derewenda, U., Kang, B. S., Bushweller, J. H., and Derewenda, Z. S. (2006) The binding of the PDZ tandem of syntenin to target proteins, *Biochemistry 45*, 3674−3683.
68. Schultz, J., Hoffmuller, U., Krause, G., Ashurst, J., Macias, M. J., Schmieder, P., Schneider-Mergener, J., and Oschkinat, H. (1998) Specific interactions between the syntrophin PDZ domain and voltage-gated sodium channels, *Nat. Struct. Biol. 5*, 19−24.
69. Handa, K., Yugawa, T., Narisawa-Saito, M., Ohno, S., Fujita, M., and Kiyono, T. (2007) E6AP-dependent degradation of DLG4/PSD95 by high-risk human papillomavirus type 18 E6 protein, *J. Virol. 81*, 1379−1389.
70. Hogan, A., Yakubchyk, Y., Chabot, J., Obagi, C., Daher, E., Maekawa, K., and Gee, S. H. (2004) The phosphoinositol 3,4-bisphosphate-binding protein TAPP1 interacts with syntrophins and regulates actin cytoskeletal organization, *J. Biol. Chem. 279*, 53717−53724.
71. Albrecht, D. E., and Froehner, S. C. (2002) Syntrophins and dystrobrevins: defining the dystrophin scaffold at synapses, *Neurosignals 11*, 123−129.
72. Li, X., and Coffino, P. (1996) High-risk human papillomavirus E6 protein has two distinct binding sites within p53, of which only one determines degradation, *J. Virol. 70*, 4509−4516.
73. Crook, T., Tidy, J. A., and Vousden, K. H. (1991) Degradation of p53 can be targeted by HPV E6 sequences distinct from those required for p53 binding and trans-activation, *Cell 67*, 547−556.
74. Muller, B. M., Kistner, U., Veh, R. W., Cases-Langhoff, C., Becker, B., Gundelfinger, E. D., and Garner, C. C. (1995) Molecular characterization and spatial distribution of SAP97, a novel presynaptic protein homologous to SAP90 and the Drosophila discs-large tumor suppressor protein, *J. Neurosci. 15*, 2354−2366.

BI700879K